2020 IEEE/RSJ International Conference on Intelligent Robots and Systems (IROS)
October 25-29, 2020, Las Vegas, NV, USA (Virtual)

A New Delayless Adaptive Oscillator for Gait Assistance

Tao Xue, Ziwei Wang, Tao Zhang, Ou Bai, Meng Zhang, and Bin Han

Abstract— **To obtain synchronized gait assistance, this paper presents a new delayless adaptive dual-oscillator (ADO) scheme to address the inherent delay issue. In the ADO structure, a new oscillator is coupled with the primitive one but the phase is adaptively feed-forward compensated. It's remarkable that the compensated phase is determined by the proposed extended phase lag observer, in which both the phase lag and phase leading can be properly estimated and eliminated in the steady and non-steady gait. Moreover, a unified exoskeleton control scheme based on ADO is further proposed to improve the gait segmentation, velocity/acceleration estimation, intention estimation, and assistance generation performances, which further enhances the assistance synergy and reduces the safety risks. Experimental results demonstrate better alignment assistance and consequently reduced muscle efforts with ADO-based assistance control.**

I. INTRODUCTION

The wearable robotic exoskeleton is a powered mechatronics system that can be used to assist elderly and disabled people with gait disorder [1], [2]. In recent years, several research institutes and companies have developed different types of exoskeletons, such as GEMS [3], SMA [4], Soft ExoSuit [5], NREL-Exo [6], etc.

Providing synchronized human-adaptive assistance is a critical issue for gait assistance. At present, there are two main solutions: one is direct sensing and the other is pattern recognition. Bioelectric based direct intention sensing, such as electromyography (EMG) [7], electroencephalograph (EEG) [8], etc., are vulnerable to interference. Moreover, the physiological model has to be calibrated individually, which seriously limits its applications. Instead, the pattern recognition method, represented by adaptive oscillator (AO), has been a popular exoskeleton control architecture due to its less sensor requirement and strong robustness [1], [2].

AO originated from the dynamic Hebbian learning rule in the nonlinear oscillator, which was first proposed by Righetti et al. to synchronize with periodic or pseudo-periodic signal [9]. Then, it was applied to human-robot synchrony control [10], where the AO is utilized to extract periodic motion features and predict assistance torque. To further enhance synchronization accuracy, Ronsse coupled the pool of adaptive oscillators to a kernel-based non-linear filter [11]. In [12], a particularly-shaped adaptive oscillator (PSAO) was proposed to effectively estimate the gait cycle, where the basic sine and cosine functions were replaced with a mapping from the phase angle to a period pattern. To improve the real-time performance, Yan designed a phase error compensator by detecting the gait event [13]. Note that the synchronization of AO-based control is through the dynamic learning law that is essentially a gradient descent method, which will introduce time delay inevitably. The following experiments show that the maximum lagged phase is up to 52.83 degrees in the acceleration process, where gait phase-based assistance will definitely produce unmatched assistance, i.e., flexion assistance in the loading phase and extension assistance for pre-swing phase. The extra resistance will hinder normal hip rotations that will increase the falling risk, especially for running activities, thus has to be well considered. Although the methods mentioned above have made significant improvements on the AO, they can not realize the delayless synchronization without external sensors. Moreover, to the best knowledge of the author, the delayless AO has not been well explored, which finally motivates this study.

To address this issue, we design a new dual-oscillator structure, where the primitive one is the typical AO while the other is coupled with feed-forward phase compensation. Based on ADO, we further propose a unified exoskeleton assistance control scheme for better gait assistance control.

II. HIP EXOSKELETON PLATFORM

A. Mechanical Design

As shown in Fig. 1, the exoskeleton has 4 degrees of freedom aligned with the hip, and two active series elastic actuator (SEA) in the flexion-extension direction while the other two passives in adduction-abduction direction. The SEA is driven by a flat brushless DC motor via a harmonic gear reducer, which has a rating output torque 12.8Nm and a maximum 60RPM velocity.

B. Electronic Design

The electrical system is responsible for data acquisition, processing, and communicating. The main control unit is a Raspberry Pi 3B platform with ubuntu mate 16.04 OS and Robot Operating System (ROS) installed. A commercial DC motor driver (Copley Accelnet Plus AE2-090-30) is adopted to realize three-loop control and instant state-feedback of actuators. Besides, a high-speed EtherCAT fieldbus with 100 Mbps is equipped and all the slave nodes communicate with a soft EtherCAT master running in the Raspberry Pi.

*This work was supported by the Beijing National Research Center for Information Science and Technology, Move Robotics Technology Company, Ltd., and the National Nature Science Foundation of China (Granted No. 51705163).

Tao Xue, Ziwei Wang and Tao Zhang are with the Department of Automation, Tsinghua University, Beijing, 100084, China. (taozhang@tsinghua.edu.cn)

Ou Bai is with the Department of Electrical and Computer Engineering, Florida International University, Miami, FL 33174, USA.

Meng Zhang is with the Move Robotics Technology Company, Ltd., Shanghai 201306, China.

Bin Han is with the School of Mechanical Science and Engineering, Huazhong University of Science and Technology, Wuhan 430074, China.

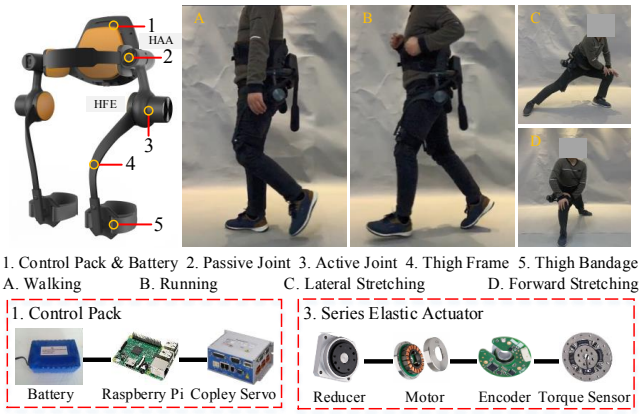

Fig. 1. Mechanical and electronic design of powered hip exoskeleton.

III. GAIT ASSISTANCE CONTROLLER

A. Assistance Control Architecture of Hip Exoskeleton

Direct AO-based control that mapped the gait phase to assistance torque has poor adaptation to nonperiodic gaits, such as cross gait with walking and stop walking. Instead, we propose a unified control scheme for various gait assistance by combining AO and active impedance control, where an improved ADO is responsible for high-level gait sensing and active impedance control for assistance generation. As shown in Fig. 2, the new ADO is proposed to synchronize the quasi-periodic hip trajectories and further obtain de-noised phase, smoothed position, velocity, and acceleration. Then, with the estimated gait intentions and velocity/acceleration, impedance shaping generates human-adaptive assistance force command to the joint controller to realize compliant assistance.

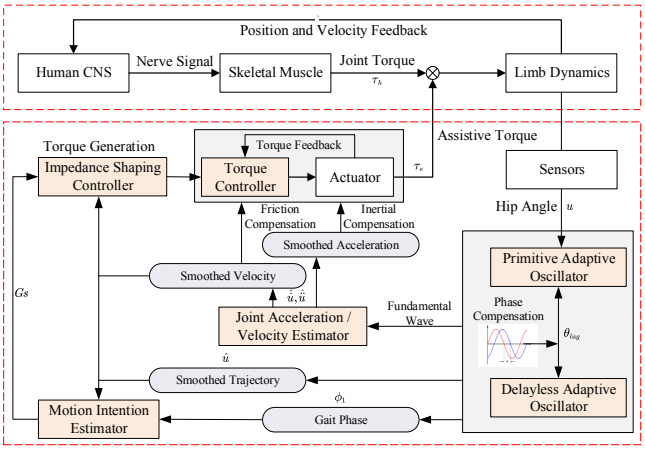

Fig. 2. Overall control architecture of powered hip exoskeleton.

B. Delayless Dual-Oscillator Scheme

(1) Typical AO: For a pseudo-periodic signal u, AO is capable of learning the features (frequency, phase, envelop, offset, etc.) by adaptive adjustment of parameters using n series harmonic oscillators[9], [10], [12]. The dynamics of AO is described as

$$\begin{cases} \hat{u} = \alpha_0 + \sum_{i=1}^{n} \alpha_i \sin(\phi_i) \\ e = u - \hat{u} \\ \dot{\alpha}_i = k_{\alpha_i} e \sin(\phi_i) \\ \dot{\phi}_i = i\omega + k_{\phi_i} e \cos(\phi_i) \\ \dot{\omega} = k_{\omega} e \cos(\phi_1) \\ \dot{\alpha}_0 = k_{\alpha_0} e \end{cases}, \tag{1}$$

where α_i, ϕ_i are the amplitude and phase of i-th oscillator, respectively. ω denotes the oscillator frequency of fundamental wave while α_0 stands for the DC bias. e is the error variable defined with the difference between u and $\hat{u}$. k_{α_0}, k_{ω} are the adjustable feedback gains of DC bias and basic frequency while $k_{\alpha_i}, k_{\phi_i}, i = 1,2,\ldots,n$ denote the amplitude and phase feedback gains of i-th oscillator. Note that ϕ_i is the phase angle of i-th harmonic wave oscillating at $i\omega$ frequency.

(2) ADO: In the AO scheme, α, ϕ, ω are updated via error feedback control, which will introduce delays inevitably. Fortunately, we propose an extended phase lag observer to eliminate the delay by lead phase compensation. Based on this intuition, we design a dual-oscillator structure, where the primitive one is the same with AO while the other is coupled with feed-forward phase compensation. The ADO is designed as

$$\begin{cases} \hat{u}_{ADO} = \alpha_0 + \alpha_1 \sin(\phi_1 + \theta_{lag}) + \sum_{i=2}^{n} \alpha_i \sin(\phi_i) \\ e = u - \hat{u} \\ \dot{\alpha}_i = k_{\alpha_i} e \sin(\phi_i) \\ \dot{\phi}_i = i\omega + k_{\phi_i} e \cos(\phi_i) \\ \dot{\omega} = k_{\omega} e \cos(\phi_1) \\ \dot{\alpha}_0 = k_{\alpha_0} e \end{cases}, \tag{2}$$

where $\hat{u}_{ADO}$ is the output of delayless dual-oscillator and θ_{lag} is the lagged phase angle of the main oscillator. Note that only the phase of the fundamental wave is compensated because the basic wave occupies the majority of the input signal. The adaptive law of compensated phase lag θ_{lag} is designed as

$$\begin{cases} e_{lag} = \cos^2(\phi_1 + \theta_{lag}) e \\ \dot{\theta}_{lag} = k_{\theta} e_{lag} \cos(\phi_1 + \theta_{lag}) \end{cases} \tag{3}$$

where k_{θ} is the positive gains determining the convergence rate and noise suppression capability of θ_{lag}. Note that the synchronization error e is not directly utilized in the θ_{lag} update but multiplied with $\cos^2(\phi_1 + \theta_{lag})$, that is because the phase lag is most significantly correlated to the errors at phases $\phi = 0, \phi = \pi$ but less at peaks or troughs, i.e., $\phi = \pi/2, \phi = 3\pi/2$. Moreover, the convergence proof of phase lag has been given as follows using the gradient descent method. The raw hip trajectory can be written as

$$u = \alpha_0^* + \alpha_1^* \sin(\phi_1^*) + \sum_{i=2}^{n} \alpha_i^* \sin(\phi_i^*) \tag{4}$$

where the superscript $*$ represents ground truth. Assume the parameter $\alpha_i, i = 1,2,\cdots,n, \phi_i, i = 2,3,\cdots,n$ are all accurately estimated, and select tracking error functions as

$$V(e_{ADO}) = \frac{1}{2}(u - \hat{u}_{ADO})^2 = \frac{1}{2}\alpha_1^*(sin(\phi_1^*) - sin(\phi_1 + \theta_{lag}))^2 \tag{5}$$

Differentitating V with respect to θ_{lag} gives

$$\nabla V(\theta_{lag}) = -e\cos(\phi_1 + \theta_{lag}) \tag{6}$$

Thus, the adpative law of θ_{lag} can be determined as Eq. (3) based on gradient descent rule

$$\dot{\theta}_{lag} = ke\cos(\phi_1 + \theta_{lag}) \tag{7}$$

where k is a positive scalar representing descent step length and k is slected as $k_\theta \cos^2(\phi_1 + \theta_{lag})$ in this paper to obtian variable step update. Therefore, the compensated phase $\phi_1 + \theta_{lag}$ will approach to the truth ϕ^* with the convergence of the synchronization error e.

C. Gait Cycle Estimation

One complete gait cycle starts from heel-strike and ends with heel-strike of the same leg, which can be divided into loading phase (LP), single support phase (SSP), pre-swing phase (PSP), and swing phase (SP)[[14]]. Usually, the gait cycle can be recognized by the aid of the foot pressure sensor or motion capture system, but it needs an extra sensing system outside the hip assistance exoskeleton. In this paper, we propose a simple gait cycle estimation method with only the hip trajectory input that can be obtained from exoskeleton joints. Since the obtained gait phase angle from the oscillator is expected to be linearly increased from 0 rad to 2π rad, four discrete gait phases can be robustly recognized with the predefined phase angle interval. Note that the cycle estimation from the AO-based approach is inaccurate due to the inherent phase lag. Instead, we use the delayless ADO scheme to address the lag issue. The phase angle interval is defined as

$$\begin{cases} \text{LP}, \pi/2 < \phi_1 + \theta_{lag} \leq \pi/2 + 0.24\pi \\ \text{SSP}, \pi/2 + 0.24\pi < \phi_1 + \theta_{lag} \leq \pi/2 + \pi \\ \text{PSP}, 3\pi/2 < \phi_1 + \theta_{lag} \leq 3\pi/2 + 0.24\pi \\ \text{SP}, \phi_1 + \theta_{lag} \leq \pi/2, \phi_1 + \theta_{lag} > 3\pi/2 + 0.24\pi \end{cases} \tag{8}$$

The LP starts at phase angle $\pi/2$, because the loading phase occurs at heel-strike around the maximum flexion point. Note that the intervals of 4 discrete phases are consistent with their duty cycle in the time domain, i.e., LP 12%, SSP 38%, another 12% for PSP, and followed by SP with 38%.

D. Joint Velocity/Acceleration Estimation

Joint velocity/acceleration can be obtained via direct numerical differentiation (DND) theoretically from the raw trajectory, however, the noise makes the DND quite challenging. In this part, based on ADO, a hip velocity/acceleration estimation method using an analytic differentiation method is introduced. The estimated velocity and acceleration are described as

$$\hat{\dot{u}} = \alpha_1 \omega \cos(\phi_1 + \theta_{lag}) \tag{9}$$

$$\hat{\ddot{u}} = -\alpha_1 \omega^2 sin(\phi_1 + \theta_{lag}) \tag{10}$$

The estimations are based on the differentiation of fundamental wave in ADO. Note that the harmonic components are not included because the adaptation to high-frequency signal is not so accurate [15].

E. Motion Intention Estimation

Stable walking is a dynamic balance process with the reciprocal transformation of kinetic energy and potential energy. The sum energy is constant theoretically for the balanced walking and will change with the gait state changes. Based on this idea, we design a novel intention estimator from the perspective of energy by introducing the orbit energy concept [16]. The dynamical equation of fundamental wave plus offset in hip oscillator can be rewritten as

$$\begin{aligned} m &= \alpha_1 \sin(\phi_1 + \theta_{lag}) + \alpha_0 \\ \dot{m} &= -\alpha_1 \sin(\phi_1 + \theta_{lag})\omega^2 \\ &= -\omega^2 m + \alpha_0 \omega^2 \end{aligned} \tag{11}$$

The orbit energy of the hip oscillator is defined as the integration of multiplying $\dot{m}$ on both sides of the Eq. (11),

$$\begin{aligned} E &= \int \dot{m}(\ddot{m} + \omega^2 m - \alpha_0 \omega^2) dt \\ &= \frac{1}{2}\dot{m}^2 + \frac{\omega^2}{2}m^2 - \alpha_0 \omega^2 m \end{aligned}, \tag{12}$$

where the first term is kinetic energy and the remaining present the potential energy. In this paper, the orbit energy of the hip oscillator is used to represent walking energy, which shows a high level during walking while relatively low level at rest. Accordingly, a variable threshold based intention estimator is developed to recognize the walking and stop walking intentions, and E_1 is the threshold for stop to walking detection and E_2 for walking to stop detection. The gait state variable Gs can be determined as

$$Gs = \begin{cases} 1, \text{if } Gs = 0 \text{ and } E > E_1 \\ 0, \text{if } Gs = 1 \text{ and } E < E_2 \end{cases} \tag{13}$$

F. Assistance Torque Generation

Based on [17], the lower-limb can be simplified as a link model rotating around the hip with rotation inertial coefficient I_h, damping coefficient b_h, and stiffness coefficient k_h. The stiffness restoring torque comes from the pull force on the limb induced by gravity, i.e., $Mgl\sin(q) \approx Mglq$, where M, g, l present the leg mass, gravity constant, and length from COG to hip while q is the hip rotation angle with its zero equilibrium point in leg vertical direction. Considering exoskeleton dynamics, the human-exoskeleton coupling dynamics can be described as

$$(I_h + I_e)\ddot{q} + (b_h + b_e)\dot{q} + (k_h + k_e)q = \tau_h + \tau_e, \tag{14}$$

where $q, \dot{q}, \ddot{q}$ denote the hip angle, hip velocity and hip acceleration, respectively. τ_h stands for the net muscle torque and τ_e is the assistance torque from exoskeleton. Similarly, I_e, b_e, k_e represents the inertial, damping, and stiffness of

exoskeleton itself. An active impedance shaping control law is designed as

$$\tau_e = I_e\ddot{q} + (b_e + b_e^d)\dot{q} + (k_e + k_e^d)q \tag{15}$$

Substituting Eq. (15) into Eq. (14), one has

$$I_h\ddot{q} + (b_h - b_e^d)\dot{q} + (k_h - k_d^d)q = \tau_h \tag{16}$$

Then, the transfer function of the coupling impedance can be described as

$$Z_h(s) = \frac{\tau_h(s)}{\dot{q}(s)} = \frac{1}{I_h s + (b_h - b_e^d) + (k_h - k_e^d)/s} \tag{17}$$

Let $b_e^d = b_h(1-A_b), k_e^d = k_h(1-A_k)$, where $0 < A_b < 1, 0 < A_k < 1$ are the assistance factor for damping and stiffness respectively. Substituting them into Eq. (17) gives

$$Z_h(s) = \frac{1}{I_h s + A_b b_h + A_k k_h/s} \tag{18}$$

From Eq. (18), we can optimize the human-exoskeleton coupling dynamical response to achieve assistance by tuning the assistance factors. With the estimated $\hat{u}, \hat{\dot{u}}, \hat{\ddot{u}}$, the hip assistance torque Eq. (15) can be rewritten as

$$\tau_e = I_e\hat{\ddot{u}} + b_e\hat{\dot{u}} + k_e\hat{u} + [b_h(1-A_b)\hat{\dot{u}} + k_h(1-A_k)\hat{u}]Gs \tag{19}$$

Note that the desired assistance torque is restricted by sensed gait state Gs, and the exoskeleton will be switched into zero torque mode automatically in stop walking gait.

IV. EXPERIMENTAL RESULTS

In this section, the ADO-based gait assistance controller is implemented in the exoskeleton with a healthy subject (male, aged 30, weight 70Kg, height 170cm). The Ethics Committee of Tsinghua University had reviewed the experimental procedure, and approved this experiment (No. 20200014). The control parameters setting are as Tab. I, where human limb parameters are taken from [17].

TABLE I
PARAMETER SETTINGS FOR ASSISTANCE CONTROL

Parameter	Value	Parameter	Value	Parameter	Value
n	2	k_{α_0}	2.0	k_{α_1}	2.0
k_{α_2}	0.1	k_{ϕ_1}	30.0	k_{ϕ_2}	50.0
k_ω	50.0	k_θ	50.0	E_1	1.8
E_2	1.5	I_e	0.24	b_e	1.0
k_e	0.2	I_h	3.38	b_h	3.50
k_h	54.70	A_b	0.77	A_k	0.99

A. Experimental Performance Index

TABLE II
PERFORMANCE INDEX

Items	AO	ADO	Reduction
RMS($u-\hat{u}$)(rad)	0.0902	**0.0704**	17.18%
RMS of Peak Delay(s)	0.0572	**0.0378**	33.92%
RMS($\dot{u}-\hat{\dot{u}}$) (rad/s)	1.29	**1.25**	3.10%
RMS($\ddot{u}-\hat{\ddot{u}}$)(rad/s/s)	7.95	**7.41**	6.80%
Stop→Walking Detection Time(s)	0.44	**0.14**	68.18%
Walking→Stop Detection Time(s)	0.48	**0.29**	39.58%

B. Gait Synchronization and Segmentation

The synchronized results of AO and ADO are presented in Fig. 3, where the gait includes both acceleration and deceleration process with frequency changes. It can be seen that ADO presents significantly improved synchronized performance than AO in both the steady and non-steady states, i.e., reducing the phase lag in steady and acceleration process, and eliminating the leading phase in deceleration process. Moreover, the estimated gait phase of ADO is linearly increased from 0 rad to 2π rad, which coincides with expected gait cycles. Note that the AO phase lag relative to ADO is even up to 0.92 rad at the rapid walking to the running point. As expected, the compensated angle in steady and acceleration process is positive for lag compensation and negative for lead compensation. It can be concluded that the proposed ADO shows better phase-locking performance in both steady and non-steady states and stronger robustness to changing gait.

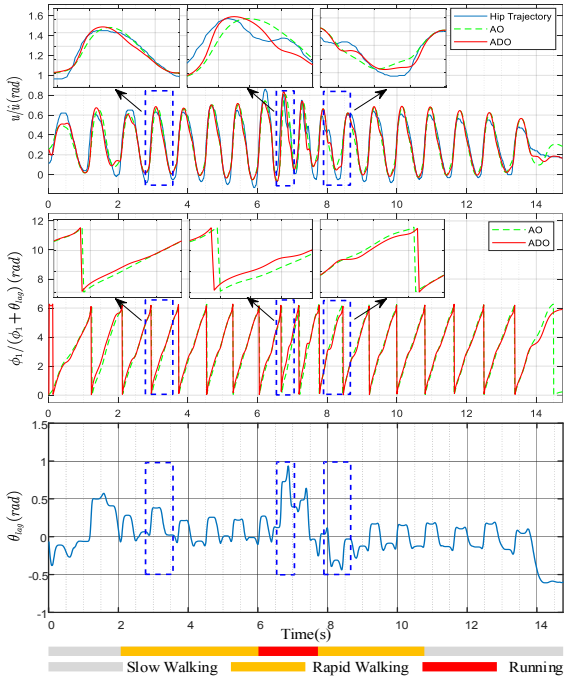

Fig. 3. Hip trajectory alignment performance using AO and ADO.

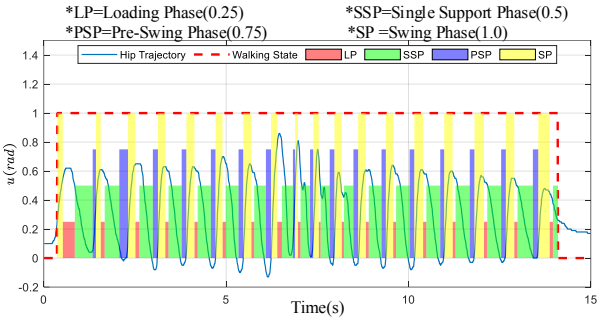

Fig. 4. 4 discrete phases in gait cycle (GC): (LP, 0-12% GC), (SSP, 12-50%), (PSP, 50-62%), and (SP, 62-100%).

The gait segmentation results are shown in Fig. 4, where LP, SSP, PSP, and SP gait stages are represented with red, green, blue, and yellow rectangles with different height. It can be seen that the LP starts at the maximum hip flexion point that is close to the heel-strike event, which implies that each complete gait cycle can be segmented accurately. Moreover, the four discrete stages are consecutively distributed in the correct order and the time duration of each stage also coincides with clinical data of gait [14].

C. Joint Velocity/Acceleration Estimation

As shown in Fig. (5), the velocity/acceleration estimations from ADO have better phase-locking performance with ground truth and consequent smaller estimation errors. As expected, the RMS of velocity and acceleration estimation errors from ADO are 1.25rad/s and 7.41rad/s/s, which are reduced by 3.10% and 6.80%, respectively. It can be concluded that ADO shows better accuracy and lower latency on the velocity and acceleration estimations.

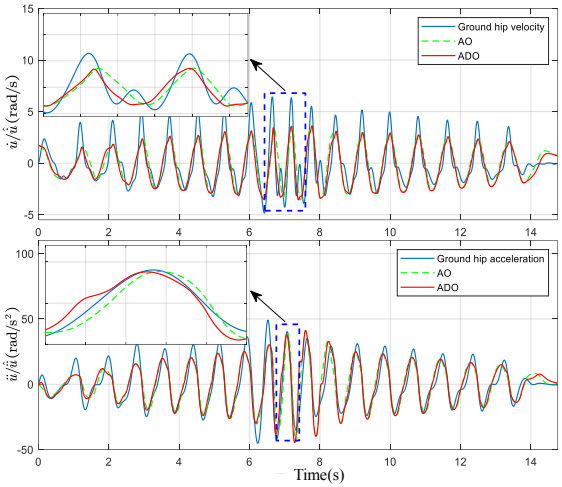

Fig. 5. Joint velocity/acceleration estimation using ADO and AO.

D. Intention Estimation

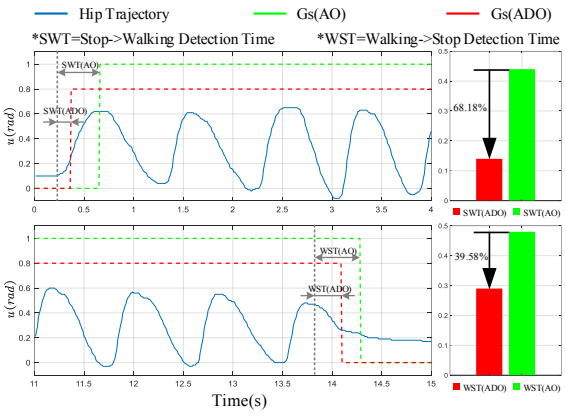

Fig. 6. Gait state detection using AO and ADO.

The dot lines in Fig. 6 are the recognized walking state variable *Gs*, which is denoted as zero in stop walking state and non-zero for walking. The stop to walking, and walking to stop can be distinguished accurately with both AO and ADO methods, but the detected time with ADO is significantly reduced when compared to AO.

E. Assistance Torque Generation

From the ADO assistance torque profile in Fig. 7, the positive flexion assistance starts at the transition point from SSP to PSP and negative extension assistance starts at from SP to LP, which is consistent with the nominal biomechanical characteristics of walking. However, it can be obtained that the AO assistance profile is not strictly aligned with phase lag or leading from the enlarged figure, which implies the extension resistance might occur in the LP and flexion resistance is possible in the PSP. The extra resistance to the hip will hinder normal hip rotations that will increase the falling risk, especially for running activities. Moreover, the zero torque mode and assistance mode are switched more timely with the proposed scheme.

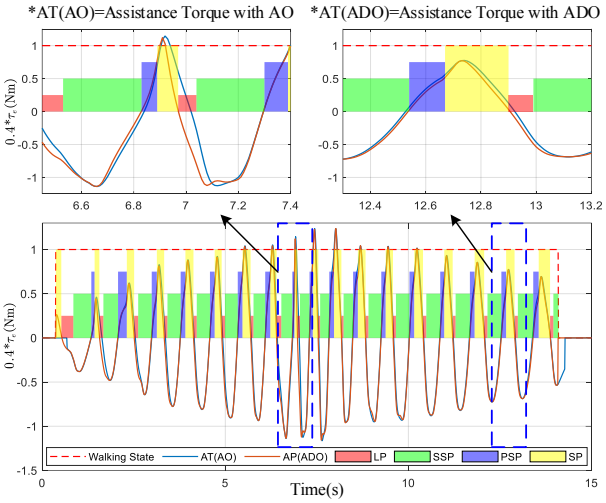

Fig. 7. Assistance torque generation using AO and ADO.

F. Assistance Evaluation

The assistance is evaluated by the muscle force that is estimated by sEMG. The sEMG electrodes are placed on the rectus femoris (RF) and biceps femoris (BF) of the left leg to evaluate the flexion and extension efforts, respectively. The sEMG is sampled in 1KHz rate and filtered with 4-order Butterworth band-pass filter (10-200Hz) to remove the movement artifacts and high-frequency noises. The moving average of the rectified sEMG signal is adopted as the activation level of muscles.

$$\beta_i = \frac{1}{N}\sum_{i=1}^{N}|x_i|/\text{MVC}, N = 150 \tag{20}$$

The subject was asked to perform 3.5Km/h, 4Km/h, 4.5Km/h, and 5Km/h treadmill walking without exoskeleton, followed by another treadmill walking session with exoskeleton on. Each experiment trial lasted 2 minutes with 15 minutes of rest to ensure sufficient time for the sEMG and

metabolic consumption level return to the baseline. To reduce the measurement uncertainties, 20 gait cycles of walking are averaged to present the true muscle activation levels.

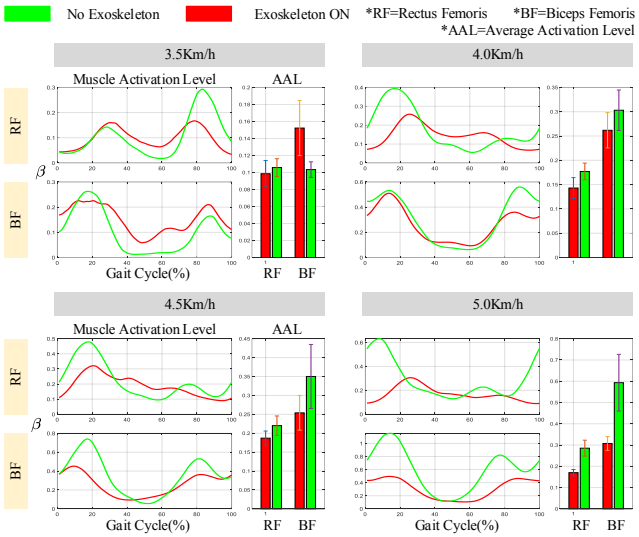

Fig. 8. Average muscle activation level in treadmill walking.

TABLE III
DECREASED MUSCLE EFFORT RATE

AAL	3.5Km/h		4.0Km/h		4.5Km/h		5.0Km/h	
	RF	BF	RF	BF	RF	BF	RF	BF
NO Exo	0.11	0.10	0.17	0.30	0.22	0.35	0.29	0.59
Exo ON	0.10	0.15	0.14	0.26	0.19	0.25	0.17	0.31
Reduction	9.0%	-50%	17.7%	13.3%	13.6%	28.6%	41.4%	47.5%

From Fig. 8 and Tab. III, it can be seen that both the activation levels of RF and BF are reduced with the exoskeleton assistance in most cases except for 3.5Km/h low-speed walking, which implies the voluntary flexion and extension torque produced by muscle has been effectively decreased. Moreover, the reduction is more increased with higher walking speed. The results also present great potential for reducing metabolic energy consumption with exoskeleton assistance.

V. CONCLUSIONS

This study proposes a new delayless adaptive dual-oscillator scheme for gait assistance to address the inherent lag issue. The alignment delay has been effectively estimated and eliminated by the proposed extended lag phase observer. Moreover, we further present a unified exoskeleton assistance control scheme based on ADO, in which the gait segmentation, intention estimation, and assistance generation are more accurate. Furthermore, the proposed control scheme has been implemented in the hip exoskeleton, and the results demonstrate unique properties, such as better alignment ability, robust intention estimation, accurate velocity/acceleration estimation, and synchronized assistance. Nevertheless, the physical experiments should be further expanded with stairs, slope walking, running, etc.

ACKNOWLEDGMENT

This work was supported by the Beijing National Research Center for Information Science and Technology, Move Robotics Technology Company, Ltd., and the National Nature Science Foundation of China (Granted No. 51705163).

REFERENCES

[1] T. Xue, Z. Wang, T. Zhang, and M. Zhang, "Adaptive oscillator-based robust control for flexible hip assistive exoskeleton," *IEEE Robotics and Automation Letters*, vol. 4, no. 4, pp. 3318–3323, Oct 2019.

[2] T. Xue, Z. Wang, T. Zhang, M. Zhang, and Z. Li, "The control system for flexible hip assistive exoskeleton," in *2018 IEEE International Conference on Robotics and Biomimetics (ROBIO)*. IEEE, 2018, pp. 697–702.

[3] K. Seo, K. Kim, Y. J. Park, J. Cho, J. Lee, B. Choi, B. Lim, Y. Lee, and Y. Shim, "Adaptive oscillator-based control for active lower-limb exoskeleton and its metabolic impact," in *2018 IEEE International Conference on Robotics and Automation (ICRA)*, May 2018, pp. 6752–6758.

[4] K. Yasuhara and Y. Miyake, "Control system for walking assist device," Feb. 1 2011, uS Patent 7,880,552.

[5] J. Kim, G. Lee, R. Heimgartner, D. A. Revi, N. Karavas, D. Nathanson, I. Galiana, A. Eckert-Erdheim, P. Murphy, D. Perry *et al.*, "Reducing the metabolic rate of walking and running with a versatile, portable exosuit," *Science*, vol. 365, no. 6454, pp. 668–672, 2019.

[6] T. Zhang, M. Tran, and H. Huang, "Admittance shaping-based assistive control of sea-driven robotic hip exoskeleton," *IEEE/ASME Transactions on Mechatronics*, vol. 24, no. 4, pp. 1508–1519, 2019.

[7] T. Kawase, T. Sakurada, Y. Koike, and K. Kansaku, "A hybrid bmi-based exoskeleton for paresis: Emg control for assisting arm movements," *Journal of neural engineering*, vol. 14, no. 1, p. 016015, 2017.

[8] S. Soekadar, M. Witkowski, C. Gómez, E. Opisso, J. Medina, M. Cortese, M. Cempini, M. Carrozza, L. Cohen, N. Birbaumer *et al.*, "Hybrid eeg/eog-based brain/neural hand exoskeleton restores fully independent daily living activities after quadriplegia," *Science Robotics*, vol. 1, no. 1, pp. eaag3296–1, 2016.

[9] L. Righetti, J. Buchli, and A. J. Ijspeert, "Dynamic hebbian learning in adaptive frequency oscillators," *Physica D: Nonlinear Phenomena*, vol. 216, no. 2, pp. 269–281, 2006.

[10] R. Ronsse, N. Vitiello, T. Lenzi, J. Van Den Kieboom, M. C. Carrozza, and A. J. Ijspeert, "Human–robot synchrony: flexible assistance using adaptive oscillators," *IEEE Transactions on Biomedical Engineering*, vol. 58, no. 4, pp. 1001–1012, 2010.

[11] R. Ronsse, T. Lenzi, N. Vitiello, B. Koopman, E. Van Asseldonk, S. M. M. De Rossi, J. Van Den Kieboom, H. Van Der Kooij, M. C. Carrozza, and A. J. Ijspeert, "Oscillator-based assistance of cyclical movements: model-based and model-free approaches," *Medical & biological engineering & computing*, vol. 49, no. 10, p. 1173, 2011.

[12] K. Seo, S. Hyung, B. K. Choi, Y. Lee, and Y. Shim, "A new adaptive frequency oscillator for gait assistance," in *2015 IEEE International Conference on Robotics and Automation (ICRA)*. IEEE, 2015, pp. 5565–5571.

[13] T. Yan, A. Parri, V. R. Garate, M. Cempini, R. Ronsse, and N. Vitiello, "An oscillator-based smooth real-time estimate of gait phase for wearable robotics," *Autonomous Robots*, vol. 41, no. 3, pp. 759–774, 2017.

[14] V. Agostini, G. Balestra, and M. Knaflitz, "Segmentation and classification of gait cycles," *IEEE Transactions on Neural Systems and Rehabilitation Engineering*, vol. 22, no. 5, pp. 946–952, 2013.

[15] R. Ronsse, S. M. M. De Rossi, N. Vitiello, T. Lenzi, M. C. Carrozza, and A. J. Ijspeert, "Real-time estimate of velocity and acceleration of quasi-periodic signals using adaptive oscillators," *IEEE Transactions on Robotics*, vol. 29, no. 3, pp. 783–791, 2013.

[16] S. Kajita, H. Hirukawa, K. Harada, and K. Yokoi, *Introduction to humanoid robotics*. Springer, 2014, vol. 101.

[17] U. Nagarajan, G. Aguirre-Ollinger, and A. Goswami, "Integral admittance shaping: A unified framework for active exoskeleton control," *Robotics and Autonomous Systems*, vol. 75, pp. 310–324, 2016.